Color control of Pr^{3+} luminescence by electron-hole recombination energy transfer in $CaTiO_3$ and $CaZrO_3$.

Supporting Information

Zoila Barandiarán,[1] Marco Bettinelli,[2] and Luis Seijo[1,*]

[1]*Departamento de Química, Instituto Universitario de Ciencia de Materiales Nicolás Cabrera, and Condensed Matter Physics Center (IFIMAC), Universidad Autónoma de Madrid, 28049 Madrid, Spain*
[2]*Dipartimento Scientifico e Tecnologico, Università di Verona, and INSTM, UdR Verona, Verona, Italy*
(Dated: June 14, 2017)

Keywords:

I. INTRODUCTION

Here we describe the details and collect the results of *ab initio* calculations on the electronic structure of Pr, Ti, and Zr ions in $CaTiO_3$:Pr^{3+} and $CaZrO_3$:Pr^{3+}. They use wave function theory and the embedded cluster approximation and have been performed with the MOLCAS package.[1]

The relativistic second-order Douglas-Kroll-Hess (DKH) many-electron Hamiltonian[2,3] has been used in all calculations. All the calculations include a first, spin-orbit coupling free step: SA-CASSCF/MS-CASPT2. In it, the spin-orbit coupling operator is removed from the Hamiltonian and state-average complete-active-space self-consistent-field variational calculations[4–6] are done on a many-electron active configurational space. The definition of the active space is case specific and will be detailed in each respective section. These SA-CASSCF calculations take care of the non-dynamic electron correlation. They are in fact multi-configurational SCF calculations in which the molecular orbital coefficients and the configuration interaction expansion coefficients are variational. Subsequently, multi-state second-order perturbation theory calculations[7–10] are performed. They take into account the dynamic correlation effects onto the ground and excited states of the embedded clusters. In these MS-CASPT2 calcualtions, the (occupied and empty) molecular orbitals optimized in the SA-CASSCF calculations are used and some selected electron shells are correlated; the latter are case specific and their choices are described in the correspondint sections. Although we call all these calculations with the general name SA-CASSCF/MS-CASPT2, some of the calculations are in fact RASSCF/RASPT2 rather than CASSCF/CASPT2: i.e., instead of configurational complete-active-spaces defined with some orbitals, restricted-active-spaces are used which are defined with larger sets of orbitals and are more flexible from the configurational point of view. In the cases where spin-orbit coupling is not basic to understand the excited states, these are all the calculations performed.

In cases where spin-orbit coupling effects are compulsory, like those involving Pr, a second step is given in order to take them into account. In the second step, the full DKH Hamiltonian is used, the atomic mean-field integrals approximation (AMFI)[11] is adopted for its spin-orbit coupling part, and restricted-active-space state-interaction spin-orbit calculations (RASSI-SO)[12] are done. The RASSI-SO calculations are a particular means to use the spin-free-state-shifting operator (SFSS)[13] in order to efficiently and effectively combine spin-orbit couplings calculated with non-dynamically correlated wave functions (e.g. CASSCF), together with spin-orbit coupling free energies calculated with dynamic correlation (e.g. CASPT2). In them, we chose the transformed CASSCF wave functions (first-order wave functions of the MS-CASPT2 method) of the spin-orbit-free states of interest as a many-electron basis, and the MS-CASPT2 energies as shifting factors.

A. $CaTiO_3$ and $CaZrO_3$ AIMP embedding potentials

The Hamiltonians of the otherwise isolated clusters are supplemented with the *ab initio* model potential (AIMP) embedding operators[14] of $CaTiO_3$ and $CaZrO_3$, which have been obtained in this work and are available from the authors[15] and in the supplementary materials. The embedding potentials have been calculated in self-consistent embedded-ions (SCEI)[16] Hartree-Fock (HF) calculations and they are made of: 1) total-ion embedding AIMPs representing Ca^{2+}, Ti^{4+}, and Zr^{4+} cations and O^{2-} anions, which are located at experimental sites of the host lattices within a cube made of $3\times3\times3$ unit cells and centered on Ca^{2+}, Ti^{4+}, or Zr^{4+}, depending on the case; and 2) a set of (4750 for Ca centered clusters and 5170 for Ti or Zr centered clusters) additional point charges situated at lattice sites and generated by the zero-multipole method of Gellé and Lepetit,[17] which closely reproduce the Ewald potential[18] within the clusters.

The experimental crystal structures of $CaTiO_3$ and $CaZrO_3$ are *Pcmn* orthorombic (Ref. 19). We used a cubic idealization of them with Ti-O and Zr-O distances equal to the experimental averages: Space group number 221, *Pm-3m* cubic, with respective lattice constants a=3.912 Å and a=4.1927 Å. Sites (a) at $(0,0,0)$ with coordination number 12 are occuppied by Ca; sites (b) at $(1/2,1/2,1/2)$ with coordination number 6 are occupied by Ti or Zr; and sites (c) at $(1/2,1/2,0)$ are occupied by O. The $CaTiO_3$ unit

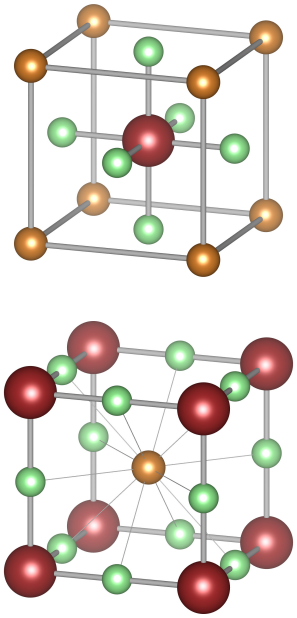

FIG. S1: Representations of the $CaTiO_3$ unit cell. Upper panel: centered on Ti (red). Lower panel: centered on Ca (orange). Oxygens are represented in green.

cell is represented in Fig. S1.

The effect of the AIMP embedding potentials of the two perovskites on the studied clusters is to include: 1) host electrostatic interactions (made of long-range point-charge or Madelung contributions and short-range charge density Coulomb contributions), 2) host-cluster exchange interactions, and 3) Pauli repulsion interactions from the host (non-orthogonality repulsive contributions due to cluster-host antisymmetry requirements). The Pauli repulsions from the O $2p$ shells as obtained in the SCEI calculations are known to be underestimated[20] and they are corrected here following the prescriptions in Ref. 20, i.e. increasing their associated projection constants in order to produce right local structures in small embedded clusters extracted from the perfect host: The use of the $CaTiO_3$ SCEI constants ($B(O_{2p})$=0.575 a.u.) gave a ground state Ti-O bond length of 2.003 Å in a CASSCF/CASPT2 calculation on the $(TiO_6Ca_8Ti_6)^{32+}$ embedded cluster and the corrected ones ($B(O_{2p})$=1.725 a.u.) give d(Ti-O)=1.957 Å, the experimental one being 1.956 Å. Accordingly, the $B(O_{2p})$ projection constants of $CaZrO_3$ have also been corrected by a factor of 3.

B. Pr^{3+} in $CaTiO_3$

Pr^{3+} is assumed to substitute for Ca^{2+} in $CaTiO_3$ and local and non-local charge compensations are assumed to take place. We have modelled the states localized in non-locally compensated Pr^{3+} defects using the $(PrO_{12})^{21-}$ embedded cluster. Non-local long-range charge compensation leads to a constant vertical shift of the electrostatic potential map that does not have any effect on the shapes of the potential energy curves nor on their relative energies. Thus, such kind of long-range charge compensation requires no manipulation of the embedding potentials of the perfect hosts. We have also calculated the energy levels of Pr^{4+} with the $(PrO_{12})^{20-}$ embedded cluster, which are useful to calculate the Pr^{3+} ionization potential in the host and Pr-to-Ti and Pr-to-Zr metal-to-metal charge transfers at the diabatic level of calculation,[21,22] For the sake of completeness, we have also calculated the energy levels of Pr^{3+} and Pr^{4+} as substitutional defects at the Ti site. For this purpose we used the $(PrO_6)^{9-}$ and $(PrO_6)^{8-}$ embedded clusters.

We performed all-electron calculations and used the following basis sets to expand the cluster molecular orbitals: Gaussian atomic natural orbital relativistic basis sets ANO-RCC for Praseodymium[23] and Oxygen,[24] with respective contractions $(25s22p15d11f4g2h)/[9s8p5d4f3g2h]$ (quadruple-zseta with polarization quality) and $(14s9p4d)/[5s4p3d]$ (quadruple-zseta with polarization without f-functions quality), plus the $3s$ and $3p$ atomic orbials of Ti^{4+} obtained in the SCEI calculations, with contraction $(20s15p)/[1s1p]$, in all Titanium atoms adjacent to the clusters; these second-neighbor basis sets are used to help enforcing the cluster-host orthogonality.[25] We performed calculations on O_h clusters using actual D_{2h} symmetry. The basis set sizes are: 551 symmetry adapted basis functions for the $(PrO_{12})^{21-}$ and $(PrO_{12})^{20-}$ clusters, and 351 symmetry adapted basis functions for the $(PrO_6)^{9-}$ and $(PrO_6)^{8-}$ clusters. The moieties showing the atoms that provide basis sets to the embedded cluster calculations are shown in Fig. S2.

The details of the SA-CASSCF/MS-CASPT2/RASSI-SO calculations on the Pr^{3+} clusters are basically identical to those used for Pr^{3+} in CaF_2 in Ref. 26. We used a CAS space made of 2 electrons in 13 molecular orbitals (1 electron in 13 MOs for Pr^{4+}) of main character Pr-4f, Pr-5d, and Pr-6s: 1 a_{2u}, 3 t_{1u}, 3 t_{2u}, 2 e_g, 3 t_{2g}, and 1 a_{1g}. We used the following state-averages for the molecular orbital optimizations: For the $4f^2$ configuration of Pr^{3+}, 1 $^3A_{2g}$ and 1 ^3E_g levels; 4 $^3T_{1g}$ and 2 $^3T_{2g}$; 3 $^1A_{1g}$, 1 $^1A_{2g}$, and 3 ^1E_g; and 2 $^1T_{1g}$ and 4 $^1T_{2g}$. For the $4f5d$ and $4f6s$ configurations of Pr^{3+}, 1 $^3A_{1u}$, 2 $^3A_{2u}$, and 3 ^3E_u levels; 6 $^3T_{1u}$ and 5 $^3T_{2u}$; 1 $^1A_{1u}$, 2 $^1A_{2u}$, and 3 ^1E_u; and 6 $^1T_{1u}$ and 5 $^1T_{2u}$. For the $4f$ configuration of Pr^{4+}, 1 $^2A_{2u}$ level; and 1 $^3T_{1u}$ and 1 $^3T_{2u}$ levels. For the $5d$ and $6s$ configurations of Pr^{4+}, 1 ^2E_g and 1 $^2A_{1g}$; and 1 $^2T_{2g}$. In the MS-CASPT2 calculations we correlated all valence electrons except those with main character Pr-4d. We used the standard IPEA value (0.25 au).[27] In the RASSI-SO calculations we included all spin singlet and triplet states for Pr^{3+}, and all spin doublets for Pr^{4+}.

The potential energy curves of the Pr^{3+} levels in the Ca-site of $CaTiO_3$ are shown in Fig. S3. The main free-ion character is used to identify the states of the $4f^2$ configuration. The states of the $4f5d(e_g)$ and $4f5d(t_{2g})$ configurations show no significant horizontal offset and no significant gap between them. This is a consequence of the very small field created at the dodecahedral Ca site.

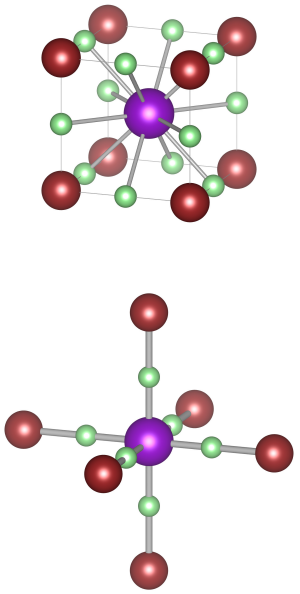

FIG. S2: Upper panel: Atoms providing basis sets to the $(PrO_{12})^{21-}$ and $(PrO_{12})^{20-}$ embedded cluster calculations. Lower panel: Atoms providing basis sets to the $(PrO_6)^{9-}$ and $(PrO_6)^{8-}$ embedded cluster calculations. Pr atoms are shown in violet, O in green, and Ti in red.

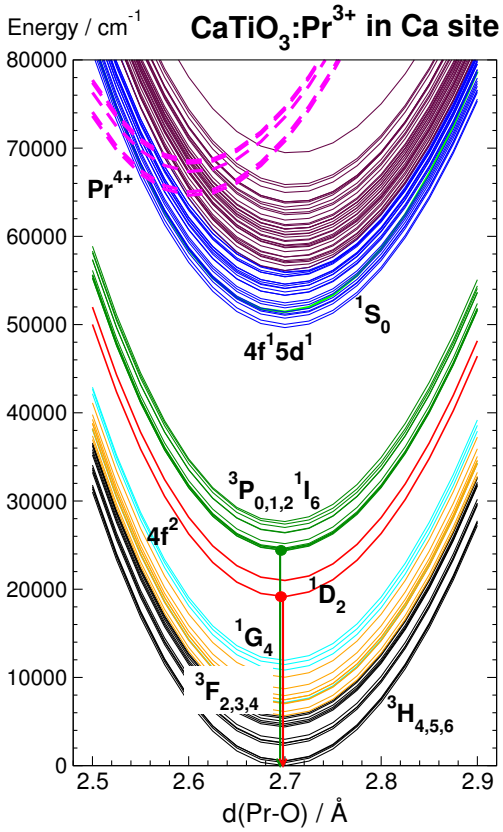

FIG. S3: Potential energy curves of Pr^{3+} and Pr^{4+} in the Ca-site of $CaTiO_3$ along the PrO_{12} breathing mode. The states of the $(PrO_{12})^{21-}$ cluster with dominant $4f^2$ configuration are shown in full lines with colors: black for main free-ion charcter $^3H_{4,5,6}$, orange for $^3F_{2,3,4}$, cyan for $^1G_4$, red for $^1D_2$, green for mixtures of $^3P_{0,1,2}$ and $^1I_6$, and bright green for $^1S_0$. The states of main configurational characters $4f5d(e_g)$ and $4f5d(t_{2g})$ are shown in blue and maroon respectively. Pr^{4+} states are shown in dashed magenta lines. Green and red emissions from the lowest level of the $^3P_{0,1,2}$ and $^1I_6$ manifold (usually referred to as $^3P_0$ emission) and the lowest $^1D_2$ level ($^1D_2$ emission), respectively, are indicated.

The assignments and spectroscopic constants of all states after spin-orbit coupling, as well as their analyses in terms of the contributions from spin-orbit coupling free states, are shown in Table S2. The results without spin-orbit coupling and without (SA-CASSCF) and with (MS-CASPT2) dynamic correlation are shown in Table S3.

The potential energy curves of the Pr^{3+} levels in the Ti-site of $CaTiO_3$ are shown in Fig. S4. In this case, the ligand field splitting of the $4f5d$ states is so large that all the $4f5d(t_{2g})$ states lie below $4f^2$ —$^1S_0$, the lowest of them overlapping the upper $4f^2$ —^3P levels. Details are shown in Tables S4 and S5.

C. Pr^{3+}/Pr^{4+} mixed valence pairs in $CaTiO_3$

D. Pr^{3+}-to-Ti^{4+} metal-to-metal charge transfer in $CaTiO_3$

Here we show the calculated metal-to-metal charge transfer (MMCT) configuration coordinate energy diagram of Pr^{3+}-Ti^{4+} pairs in $CaTiO_3$, i.e. the energy diagram with the states of the Pr^{3+}-Ti^{4+} and Pr^{4+}-Ti^{3+} pairs in $CaTiO_3$. We calculated the MMCT diagram at the diabatic level[21,22] and corrected it by shifting the diabatic energies of the Pr^{4+}-Ti^{3+} pair at d_{Pr-O}=2.700 Å and d_{Ti-O}=1.956 Å (relative to the Pr^{3+}-Ti^{4+} ground state) to their correct adiabatic values as calculated in the $(PrO_{12}Ti_8O_{24})^{37-}$ cluster embedded in $CaTiO_3$. In this way, for this particular structure we remove the errors inherent to the approximation of considering the electron transfer as the addition of an independent Pr^{3+} ionization, plus an independent electron attachment on Ti^{4+}, plus a change of electrostatic interactions. For other structures, this procedure assumes the approximation that the energy correction is the same.

In the adiabatic calculations, we used the $(PrO_{12}Ti_8O_{24})^{37-}$ cluster shown in Fig. S6 and performed SA-CASSCF/MS-CASPT2 calculations. These are all-electron calculations with the following basis sets to expand the cluster molecular orbitals: Gaussian atomic natural orbital relativistic basis sets ANO-RCC for Praseodymium,[23] Titanium,[28] and Oxygen,[24] with respective contractions $(25s22p15d11f4g)/[7s6p3d2f1g]$ (double-zseta with polarization quality), $(21s15p10d)/[5s4p2d]$ (double-zseta quality), and $(14s9p4d)/[3s2p1d]$ (double-zseta with polarization quality). We performed the calculations on the O_h cluster using actual D_{2h} symmetry with a total of 783 symmetry adapted basis functions. We used a CAS

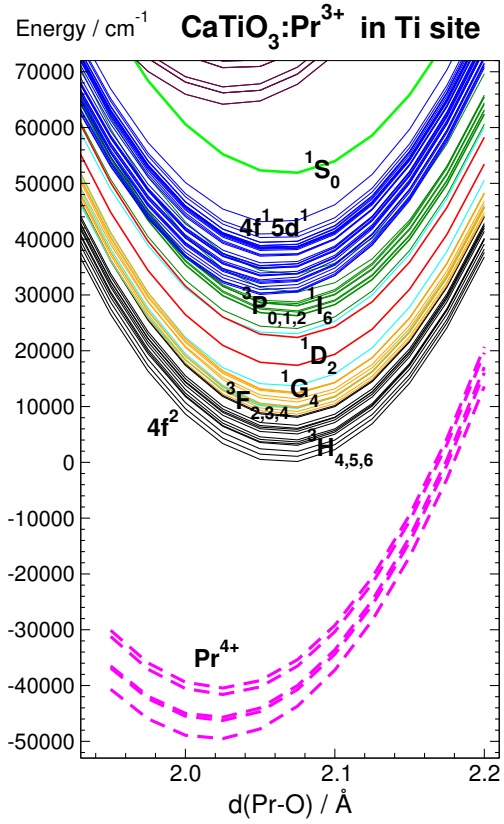

FIG. S4: Potential energy curves of Pr^{3+} and Pr^{4+} in the Ti-site of $CaTiO_3$ along the PrO_6 breathing mode. The states of the $(PrO_6)^{9-}$ cluster with dominant $4f^2$ configuration are shown in full lines with colors: black for main free-ion charcter $^3H_{4,5,6}$, orange for $^3F_{2,3,4}$, cyan for $^1G_4$, red for $^1D_2$, green for mixtures of $^3P_{0,1,2}$ and $^1I_6$, and bright green for $^1S_0$. The states of main configurational characters $4f\,5d(t_{2g})$ are shown in blue. Impurity-trapped-exciton states are shown in maroon. Pr^{4+} states are shown in dashed magenta lines.

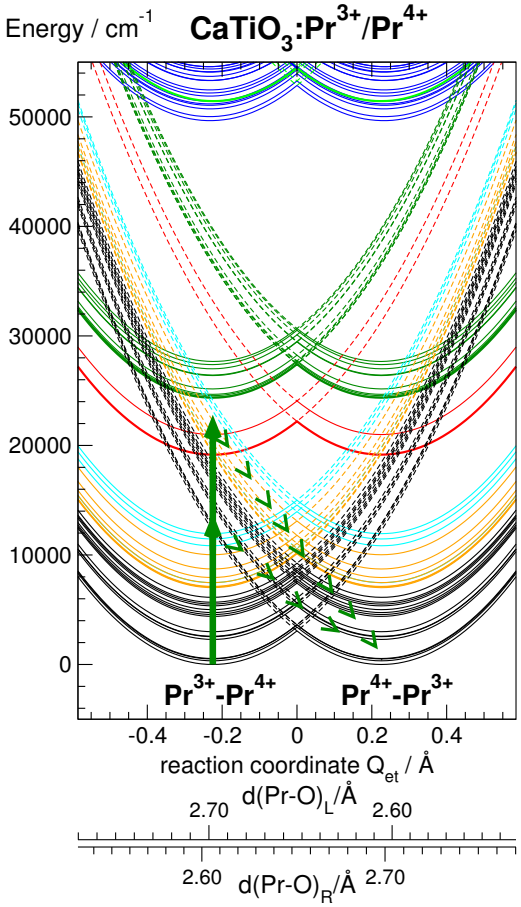

FIG. S5: Potential energy curves along the electron transfer reaction coordinate of the mixed valence pair Pr^{3+}/Pr^{4+} in $CaTiO_3$.

space made of 2 electrons in 27 MOs of main character Pr-4f and Ti-3d g for spin singlet and triplet u states, and 2 electrons in 27 MOs of main character Pr-4f and Ti-3d u for spin singlet and triplet g states. And we used the following state-averages for the MO optimizations. For the $4f^2$ configuration of Pr^{3+} and the g MMCT states: 13 $^3A_{1g}$, $^3A_{2g}$, and ^3E_g states (in actual ^3A_g D_{2h} irrep); 15 $^3T_{1g}$ and $^3T_{2g}$ levels (in actual $^3B_{1g}$, $^3B_{2g}$, and $^3B_{3g}$ D_{2h} irreps); 18 $^1A_{1g}$, $^1A_{2g}$, and ^1E_g states (in actual ^1A_g D_{2h} irrep); and 12 $^1T_{1g}$ and $^1T_{2g}$ levels (in actual $^1B_{1g}$, $^1B_{2g}$, and $^1B_{3g}$ D_{2h} irreps). For the u MMCT states: 35 $^3A_{1u}$, $^3A_{2u}$, and ^3E_u states (in actual ^3A_u D_{2h} irrep); 35 $^3T_{1u}$ and $^3T_{2u}$ levels (in actual $^3B_{1u}$, $^3B_{2u}$, and $^3B_{3u}$ D_{2h} irreps); 35 $^1A_{1u}$, $^1A_{2u}$, and ^1E_u states (in actual ^1A_u D_{2h} irrep); and 35 $^1T_{1u}$ and 5 $^1T_{2u}$ levels (in actual $^1B_{1u}$, $^1B_{2u}$, and $^1B_{3u}$ D_{2h} irreps). In the MS-CASPT2 calculations we correlated all valence electrons except those with main character Pr-4d. We did not include spin-orbit coupling in these calculations. The resulting MMCT diagram for $CaTiO_3$:Pr^{3+}/Ti^{4+} is shown in

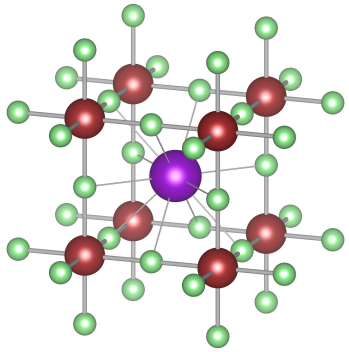

FIG. S6: $PrO_{12}Ti_8O_{24}$ moiety. Pr is shown in violet, O in green, and Ti in red.

Fig. S7. The Pr-to-Ti electron transfer reaction coordinate is represented in Fig. S8.

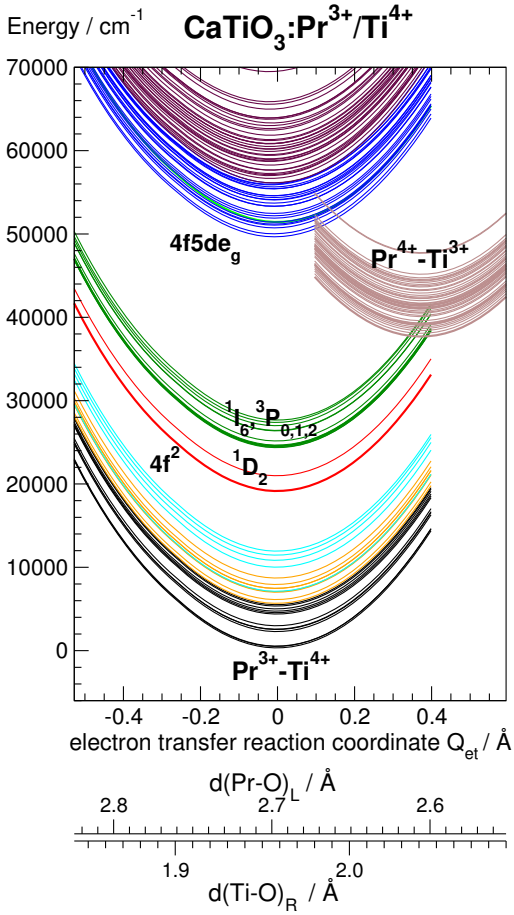

FIG. S7: MMCT diagram of Pr^{3+}/Ti^{4+} pairs in $CaTiO_3$.

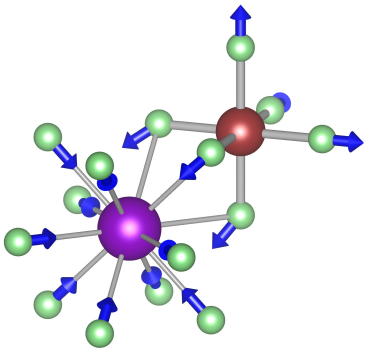

FIG. S8: Pr-to-Ti electron transfer reaction coordinate.

E. Ligand-to-metal charge transfer in $CaTiO_3$ and $CaZrO_3$

For the LMCT states O-to-Ti in $CaTiO_3$ and O-to-Zr in $CaZrO_3$, we performed SA-CASSCF/MS-CASPT2 calculations on the $(TiO_6Ca_8Ti_6)^{32+}$ and $(ZrO_6Ca_8Zr_6)^{32+}$ clusters (as represented in Fig. S9) embedded in their respective hosts.

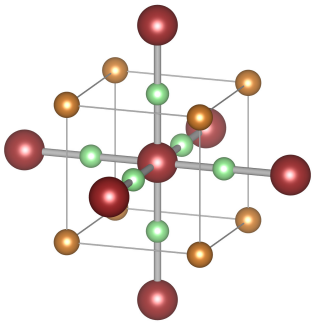

FIG. S9: $(TiO_6Ca_8Ti_6)^{32+}$cluster. Ti is shown in red, O in green, and Ca in gold.

We did all-electron calculations with Gaussian atomic natural orbital relativistic basis sets ANO-RCC for Titanium,[28] Zirconium,[28] Calcium,[29] and Oxygen.[24] For the innermost Ti atoms we used the contraction $(21s15p10d6f4g)/[7s6p4d3f2g]$ (quadruple-zeta with polarization quality) and for the outermost Ti atoms $(21s15p10d)/[5s4p2d]$ (double-zeta quality except for f functions); equivalently, for the innermost Zr atoms $(21s18p13d6f4g)/[8s7p5d3f2g]$ (quadruple-zeta with polarization quality) and for the outermost Zr atoms $(21s18p13d)/[6s5p3d]$ (double-zeta quality except for f functions); for O $(14s9p4d)/[5s4p3d]$ (quadruple-zeta with polarization quality except for f functions); and for Ca $(20s16p6d)/[5s3p2d]$ (double-zeta with polarization quality). We performed calculations on O_h clusters using actual D_{2h} symmetry. The basis set sizes are: 630 symmetry adapted basis functions for the $(TiO_6Ca_8Ti_6)^{32+}$ cluster and 693 symmetry adapted basis functions for the $(ZrO_6Ca_8Zr_6)^{32+}$ cluster.

In order to make a choice of active orbitals for the CASSCF calculations, we did a preliminary Hartree-Fock calculation on $(TiO_6Ti_6)^{16+}$ at d_{Ti-O}=1.95 Å. This gives the following frontier orbital energies (in hartree): occupied MOs with dominant character O_{2p}: $a_{1g}(O_{2p\sigma})$=–0.436, $e_g(O_{2p\sigma})$=–0.416, $t_{1u}(O_{2p\sigma})$=–0.379, $t_{2g}(O_{2p\pi})$=–0.378, $t_{2u}(O_{2p\pi})$=–0.312, $t_{1u}(O_{2p\pi})$=–0.305, $t_{1g}(O_{2p\pi})$=–0.281; and unoccupied MOs with dominant character of Ti: $t_{2g}(Ti_{3d})$=0.301, $e_g(Ti_{3d})$=0.401, $a_{1g}(Ti_{4s})$=0.553, $t_{1u}(Ti_{4p})$=0.661. This suggest that the lowest $O_{2p}\rightarrow$Ti LMCT excitations will be $t_{1g}(O_{2p\pi})\rightarrow t_{2g}(Ti_{3d})$, $t_{1u}(O_{2p\pi})\rightarrow t_{2g}(Ti_{3d})$, and $t_{2u}(O_{2p\pi})\rightarrow t_{2g}(Ti_{3d})$. This was confirmed with MS-RASPT2 calculations with a restricted-active-space RAS in which one hole only was allowed in the 18 MOs with dominant character O_{2p} and one electron only was allowed in the 3 MOs t_{2g} with dominant character Ti_{3d}. In such calculations, the mentioned LMCT excitations lie in 40600-49800 cm^{-1} whereas all others are in the range 57500-78300 cm^{-1}.

Accordingly, we used a configurational CAS in which: for

spin singlet ant triplet g LMCT states, 6 electrons are distributed in all possible ways (compatible with spin and spatial irrep) in the 6 MOs of main characters $t_{1g}(O_{2p\pi})$ and $t_{2g}(Ti_{3d}$ or $Zr_{4d})$; and for spin singlet ant triplet u LMCT states, 12 electrons are distributed in the 9 MOs of main characters $t_{1u}(O_{2p\pi})$, $t_{2u}(O_{2p\pi})$, and $t_{2g}(Ti_{3d}$ or $Zr_{4d})$. We used the following state-averages for the MO optimizations: $1\,^1A_{1g}$, $1\,^1A_{2g}$, and $1\,^1E_g$ levels; $1\,^1T_{1g}$ and $1\,^1T_{2g}$; $1\,^1A_{1u}$, $1\,^1A_{2u}$, and $2\,^1E_u$; $2\,^1T_{1u}$ and $2\,^1T_{2u}$; $1\,^3A_{2g}$ and $1\,^3E_g$; $1\,^3T_{1g}$ and $1\,^3T_{2g}$; $1\,^3A_{1u}$, $1\,^3A_{2u}$, and $2\,^3E_u$; and $2\,^1T_{1u}$ and $2\,^1T_{2u}$. In the MS-CASPT2 calculations we correlated all valence electrons. We did not include spin-orbit coupling in these calculations. The results are summarized in Table S1.

TABLE S1: Spectroscopic constants of the O-to-Ti and O-to-Zr LMCT states after MS-CASPT2 calculations on the $(TiO_6Ca_8Ti_6)^{32+}$ and $(ZrO_6Ca_8Zr_6)^{32+}$ clusters embedded in $CaTiO_3$ and $CaZrO_3$ respectively. Ti–O and Zr–O equilibrium distances $d_{Ti-O,e}$ and $d_{Zr-O,e}$ (Å), breathing mode harmonic vibrational frequencies $\omega_{a_{1g}}$ (cm^{-1}), and minimum-to-minimum transition energies T_e (cm^{-1}). The allowed absorptions ($^1A_{1g}\rightarrow{}^1T_{1u}$) are highlighted.

Level	$d_{Ti-O,e}$	$\omega_{a_{1g}}$	T_e	$d_{Zr-O,e}$	$\omega_{a_{1g}}$	T_e
		$CaTiO_3$			$CaZrO_3$	
Ground state						
$1\,^1A_{1g}$	1.957	794	0	2.105	775	0
LMCT states						
$1\,^1A_{2g}$	2.001	775	20720	2.143	744	43360
$1\,^1E_g$	2.000	786	21110	2.139	732	44010
$1\,^3E_g$	1.999	777	23490	2.145	763	44960
$1\,^3A_{2g}$	1.999	775	23790	2.145	761	45680
$1\,^1T_{1g}$	1.995	793	26650	2.140	765	48910
$1\,^1T_{2g}$	1.995	793	26720	2.139	764	48720
$1\,^1E_u$	2.006	817	27240	2.147	505	48430
$1\,^3E_u$	2.006	800	27790	2.150	830	48810
$1\,^3T_{2g}$	1.996	791	27830	2.141	767	50550
$1\,^3T_{1g}$	1.996	792	28030	2.141	769	50020
$1\,^1A_{1u}$	2.006	801	28620	2.152	767	50530
$2\,^3E_u$	2.007	803	29200	2.150	965	50050
$1\,^3T_{1u}$	2.005	807	29320	2.147	736	49410
$1\,^3A_{1u}$	2.006	801	29630	2.152	771	51290
$1\,^1A_{2u}$	2.008	801	29800	2.150	771	49650
$2\,^1E_u$	2.010	777	28900	2.155	711	49450
$1\,^1T_{1u}$	**2.004**	**783**	**29470**	**2.145**	**782**	**49290**
$2\,^1T_{2u}$	2.003	746	30410	2.147	898	51130
$2\,^3T_{2u}$	2.001	724	30500	2.148	763	50620
$3\,^1T_{1u}$	**2.006**	**812**	**30710**	**2.147**	**732**	**52800**
$1\,^3A_{2u}$	2.008	801	30890	2.151	771	50910
$3\,^3T_{1u}$	2.009	803	31110	2.145	668	53130
$4\,^1T_{2u}$	2.004	789	31140	2.149	688	55140
$4\,^3T_{2u}$	2.008	799	31690	2.162	755	54540

* Corresponding author; Electronic address: luis.seijo@uam.es

1 Karlström, G.; Lindh, R.; Malmqvist, P. A.; Roos, B. O.; Ryde, U.; Veryazov, V.; Widmark, P. O.; Cossi, M.; Schimmelpfennig, B.; Neogrady, P.; Seijo, L. *Comput. Mater. Sci.* **2003**, *28*, 222–239.

2 Douglas, M.; Kroll, N. M. *Ann. Phys. (N.Y.)* **1974**, *82*, 89–155.

3 Hess, B. A. *Phys. Rev. A* **1986**, *33*, 3742–3748.

4 Roos, B. O.; Taylor, P. R.; Siegbahn, P. E. M. *Chem. Phys.* **1980**, *48*, 157–173.

5 Siegbahn, P. E. M.; Heiberg, A.; Roos, B. O.; Levy, B. *Phys. Scr.* **1980**, *21*, 323–327.

6 Siegbahn, P. E. M.; Heiberg, A.; Almlöf, J.; Roos, B. O. *J. Chem. Phys.* **1981**, *74*, 2384–2396.

7 Andersson, K.; Malmqvist, P.-A.; Roos, B. O.; Sadlej, A. J.; Wolinski, K. *J. Phys. Chem.* **1990**, *94*, 5483–5488.

8 Andersson, K.; Malmqvist, P.-A.; Roos, B. O. *J. Chem. Phys.* **1992**, *96*, 1218–1226.

9 Zaitsevskii, A.; Malrieu, J.-P. *Chem. Phys. Lett.* **1995**, *233*, 597–604.

10 Finley, J.; Malmqvist, P.-A.; Roos, B. O.; Serrano-Andrés, L. *Chem. Phys. Lett.* **1998**, *288*, 299–306.

11 Hess, B. A.; Marian, C. M.; Wahlgren, U.; Gropen, O. *Chem. Phys. Lett.* **1996**, *251*, 365–371.

12 Malmqvist, P. A.; Roos, B. O.; Schimmelpfennig, B. *Chem. Phys. Lett.* **2002**, *357*, 230–240.

13 Llusar, R.; Casarrubios, M.; Barandiarán, Z.; Seijo, L. *J. Chem. Phys.* **1996**, *105*, 5321–5330.

14 Barandiarán, Z.; Seijo, L. *J. Chem. Phys.* **1988**, *89*, 5739–5746.

15 Detailed embedding AIMP data libraries in electronic format are available from the authors upon request or directly at the address http://www.uam.es/quimica/aimp/-Data/AIMPLibs.html. See also Ref. 1.

16 Seijo, L.; Barandiarán, Z. *J. Chem. Phys.* **1991**, *94*, 8158.

17 Gellé, A.; Lepetit, M.-B. *J. Chem. Phys.* **2008**, *128*, 244716–1–8.

18 Ewald, P. P. *Ann. Phys.* **1921**, *369*, 253–287.

19 Koopmans, H.; van de Velde, G.; Gellings, P. *Acta Crystallogr.* **1983**, *C39*, 1323–1325.

20 Pascual, J. L.; Barros, N.; Barandiarán, Z.; Seijo, L. *J. Phys. Chem. A* **2009**, *113*, 12454.

21 Barandiarán, Z.; Meijerink, A.; Seijo, L. *Phys. Chem. Chem. Phys.* **2015**, *17*, 19874.

22 Barandiarán, Z.; Seijo, L. *J. Chem. Phys.* **2015**, *143*, 144702.

23 B. O. Roos, R. Lindh, P. A. Malmqvist, V. Veryazov, P. O. Widmark,; Borin, A. C. *J. Phys. Chem. A* **2008**, *112*, 11431–11435.

24 Roos, B. O.; Lindh, R.; Malmqvist, P. A.; Veryazov, V.; Widmark, P. O. *J. Phys. Chem. A* **2004**, *108*, 2851–2858.

25 Pascual, J. L.; Seijo, L. *J. Chem. Phys.* **1995**, *102*, 5368.

26 Krośnicki, M.; Kedziorski, A.; Seijo, L.; Barandiarán, Z. *J. Phys. Chem. A* **2014**, *118*, 358–68.

27 G. Ghigo, B. O. Roos,,; P.-Å. Malmqvist, *Chem. Phys. Lett.* **2004**, *396*, 142.

28 Roos, B. O.; Lindh, R.; Malmqvist, P. A.; Veryazov, V.; Widmark, P. O. *J. Phys. Chem. A* **2005**, *109*, 6575–6579.

29 Roos, B. O.; Veryazov, V.; Widmark, P. O. *Theor. Chim. Acta* **2003**, *111*, 345–351.

TABLE S2: Spectroscopic constants and analyses of the spin-orbit wave functions of the electronic states of Pr^{3+} and Pr^{4+} at the Ca site of $CaTiO_3$. Pr–O equilibrium distances $d_{Pr-O,e}$ (Å), breathing mode harmonic vibrational frequencies $\omega_{a_{1g}}$ (cm^{-1}), and minimum-to-minimum transition energies T_e (cm^{-1}). The analysis of the spin-orbit wave functions corresponds to d_{Pr-O}=2.7 Å. Manifold averages and mean square deviations are indicated when meaningful. See Fig. S3.

State		$d_{Pr-O,e}$	$\omega_{a_{1g}}$	T_e	weights (%) of terms larger than 10%							
Pr^{3+}												
					$4f^2$ manifold							
					$\langle d_{Pr-O,e}\rangle$=2.698±0.002; $\langle \omega_{a_{1g}}\rangle$=498±2							
$^3H_4$	$1\,E_g$	2.698	497	0	57.09	$1\,^3T_{2g}$	37.12	$1\,^3T_{1g}$				
	$1\,T_{1g}$	2.698	496	330	60.50	$1\,^3T_{2g}$	27.18	$2\,^3T_{1g}$				
	$1\,A_{1g}$	2.699	495	510	92.13	$2\,^3T_{1g}$						
	$1\,T_{2g}$	2.698	498	540	73.45	$1\,^3T_{1g}$	18.85	$1\,^3E_g$				
$^3H_5$	$2\,E_g$	2.698	497	2290	55.28	$1\,^3T_{1g}$	24.85	$1\,^3T_{2g}$	19.30	$2\,^3T_{1g}$		
	$2\,T_{2g}$	2.698	496	2540	58.92	$1\,^3T_{2g}$	23.35	$2\,^3T_{1g}$	12.15	$1\,^3E_g$		
	$2\,T_{1g}$	2.699	496	2580	66.14	$2\,^3T_{1g}$	29.23	$1\,^3T_{2g}$				
	$3\,T_{1g}$	2.698	497	2990	67.54	$1\,^3T_{1g}$	27.86	$1\,^3E_g$				
$^3H_6$	$1\,A_{2g}$	2.698	497	4390	98.27	$1\,^3T_{2g}$						
	$2\,A_{1g}$	2.698	498	4560	95.66	$1\,^3T_{1g}$						
	$3\,T_{2g}$	2.698	496	4740	36.51	$1\,^3T_{2g}$	36.04	$2\,^3T_{1g}$	13.23	$1\,^3T_{1g}$		
	$3\,E_g$	2.699	495	5000	76.85	$2\,^3T_{1g}$	16.57	$1\,^3T_{2g}$				
	$4\,T_{1g}$	2.698	497	5350	61.98	$1\,^3E_g$	24.46	$1\,^3T_{1g}$				
	$4\,T_{2g}$	2.698	498	5520	33.73	$1\,^3E_g$	29.99	$2\,^3T_{1g}$	15.69	$2\,^3T_{2g}$	14.79	$3\,^3T_{1g}$
$^3F_2$	$4\,E_g$	2.699	502	5680	56.25	$3\,^3T_{1g}$	40.66	$2\,^3T_{2g}$				
	$5\,T_{2g}$	2.699	499	6130	38.85	$2\,^3T_{2g}$	25.67	$1\,^3E_g$	15.09	$3\,^3T_{1g}$		
$^3F_{3,4}$	$2\,A_{2g}(^3F_3)$	2.698	500	7014	98.46	$2\,^3T_{2g}$						
	$5\,T_{1g}$	2.699	501	7080	73.65	$2\,^3T_{2g}$	24.01	$3\,^3T_{1g}$				
$^1G_4$	$3\,A_{1g}(^1G_4)$	2.698	499	7120	56.69	$1\,^1A_{1g}$	39.87	$3\,^3T_{1g}$				
	$6\,T_{2g}$	2.699	502	7470	67.17	$3\,^3T_{1g}$	22.00	$2\,^3T_{2g}$				
	$5\,E_g$	2.699	500	7470	35.38	$2\,^3T_{2g}$	33.16	$1\,^1E_g$	29.00	$3\,^3T_{1g}$		
	$6\,T_{1g}$	2.699	501	7940	58.47	$3\,^3T_{1g}$	21.58	$1\,^1T_{1g}$	18.56	$2\,^3T_{2g}$		
	$7\,T_{2g}$	2.698	497	8720	66.91	$1\,^3A_{2g}$	22.36	$1\,^1T_{2g}$				
	$4\,A_{1g}(^3F_4)$	2.698	500	10029	59.84	$3\,^3T_{1g}$	38.64	$1\,^1A_{1g}$				
	$6\,E_g$	2.699	498	10840	64.49	$1\,^1E_g$	22.35	$2\,^3T_{2g}$	12.66	$3\,^3T_{1g}$		
	$7\,T_{1g}$	2.699	497	11460	75.81	$1\,^1T_{1g}$	15.85	$3\,^3T_{1g}$				
	$8\,T_{2g}$	2.698	498	11960	73.29	$1\,^1T_{2g}$	15.18	$1\,^3A_{2g}$				
$^1D_2$	**$7\,E_g$**	2.698	502	**19170**	92.57	$2\,^1E_g$						
	$9\,T_{2g}$	2.698	497	20990	88.38	$2\,^1T_{2g}$	10.14	$4\,^3T_{1g}$				
$^1I_6, ^3P_0$	**$5\,A_{1g}$**	2.698	499	**24360**	61.21	$2\,^1A_{1g}$	38.22	$4\,^3T_{1g}$				
	$8\,E_g$	2.698	507	24410	98.70	$3\,^1E_g$						
$^3P_0, ^1I_6$	$6\,A_{1g}$	2.698	500	24550	60.72	$4\,^3T_{1g}$	38.54	$2\,^1A_{1g}$				
	$3\,A_{2g}$	2.698	500	24670	99.76	$1\,^1A_{2g}$						
$^3P_1$	$8\,T_{1g}$	2.698	503	25160	100.00	$4\,^3T_{1g}$						
$^3P_2$	$9\,E_g$	2.698	503	26380	93.69	$4\,^3T_{1g}$						
	$10\,T_{2g}$	2.698	498	26430	80.27	$4\,^3T_{1g}$	10.21	$3\,^1T_{2g}$				
	$9\,T_{1g}$	2.699	485	27000	99.80	$2\,^1T_{1g}$						
	$11\,T_{2g}$	2.699	494	27380	89.30	$3\,^1T_{2g}$						
	$12\,T_{2g}$	2.697	496	27670	99.14	$4\,^1T_{2g}$						
$^1S_0$	$7\,A_{1g}$	2.698	497	51440	98.94	$3\,^1A_{1g}$						
					$4f5de_g$ submanifold							
					$\langle d_{Pr-O,e}\rangle$=2.802±0.002; $\langle \omega_{a_{1g}}\rangle$=488±1							
	$1\,T_{2u}$	2.701	488	49650	80.44	$1\,^1T_{2u}$	10.72	$1\,^3T_{2u}$				
	$1\,E_u$	2.702	488	50020	63.07	$1\,^1E_u$	25.59	$1\,^3T_{1u}$				
	$2\,T_{2u}$	2.701	488	50730	58.34	$1\,^3T_{1u}$	20.00	$1\,^3T_{2u}$	16.52	$2\,^1T_{2u}$		
	$2\,E_u$	2.701	488	51050	42.35	$1\,^3T_{1u}$	18.98	$1\,^1E_u$	17.36	$1\,^3T_{2u}$	15.97	$2\,^3T_{2u}$
	$1\,T_{1u}$	2.702	487	51180	45.38	$1\,^3T_{1u}$	30.66	$1\,^1T_{1u}$	10.25	$1\,^3T_{2u}$		
	$1\,A_{2u}$	2.701	486	51420	88.93	$1\,^3T_{2u}$						
	$1\,A_{1u}$	2.702	487	51890	61.44	$2\,^3T_{1u}$	32.46	$1\,^3T_{1u}$				
	$3\,T_{2u}$	2.702	488	52170	28.68	$1\,^3E_u$	23.51	$1\,^3T_{2u}$	15.88	$2\,^3T_{2u}$	15.31	$2\,^1T_{2u}$
	$2\,T_{1u}$	2.702	489	52460	36.08	$1\,^3E_u$	35.18	$2\,^3T_{1u}$	10.39	$2\,^3T_{2u}$		
	$3\,T_{1u}$	2.702	487	53310	43.36	$1\,^3T_{2u}$	22.71	$1\,^1T_{1u}$	20.58	$2\,^3T_{2u}$		

4 T_{2u}	2.701	487	53320	32.57	1 $^3T_{2u}$	22.09	1 $^3T_{1u}$	15.00	1 $^1T_{2u}$	10.89	1 ^3E_u
2 A_{1u}	2.703	490	53700	59.49	1 $^3T_{1u}$	22.00	2 $^3T_{1u}$	17.43	1 $^1A_{1u}$		
3 E_u	2.701	486	54080	67.58	1 $^3T_{2u}$	19.11	1 $^3T_{1u}$				
4 T_{1u}	2.703	493	54120	39.26	1 $^1T_{1u}$	37.75	1 $^3T_{1u}$				
5 T_{1u}	2.702	488	54360	42.91	2 $^3T_{1u}$	16.79	1 $^3T_{2u}$	16.02	1 ^3E_u	13.84	1 $^3T_{1u}$
5 T_{2u}	2.703	489	54580	34.07	2 $^1T_{2u}$	28.21	1 ^3E_u	13.25	1 $^3T_{1u}$		
4 E_u	2.702	490	54580	44.99	2 $^3T_{2u}$	24.18	2 $^3T_{1u}$	15.49	1 ^1E_u		
2 A_{2u}	2.703	489	55400	73.37	2 $^3T_{2u}$	16.00	3 $^3T_{2u}$	10.25	1 $^3T_{2u}$		
6 T_{1u}	2.702	488	55430	43.47	2 $^3T_{2u}$	29.43	1 ^3E_u	13.41	1 $^3T_{2u}$		
6 T_{2u}	2.702	489	55640	62.52	2 $^3T_{2u}$	12.50	2 $^1T_{2u}$				
5 E_u	2.707	481	55890	62.87	2 ^1E_u	11.70	3 $^3T_{2u}$	11.57	3 $^3T_{1u}$		
7 T_{2u}	2.702	488	56110	63.12	2 $^3T_{1u}$	12.40	1 ^3E_u				
7 T_{1u}	2.707	493	56660	37.76	3 $^3T_{1u}$	14.81	1 $^3A_{1u}$	13.37	2 $^1T_{1u}$	12.13	4 $^3T_{1u}$
$4f\,5dt_{2g}$ submanifold											
$\langle d_{\mathrm{Pr-O},e}\rangle$=2.708±0.001; $\langle \omega_{a_{1g}}\rangle$=496±2											
3 A_{1u}	2.707	498	55960	54.23	1 $^1A_{1u}$	23.17	3 $^3T_{1u}$	16.08	2 $^3T_{1u}$		
6 E_u	2.703	504	56130	63.62	2 $^3T_{1u}$	22.22	2 $^3T_{2u}$				
8 T_{2u}	2.708	496	57000	46.83	4 $^3T_{1u}$	42.13	2 ^3E_u				
9 T_{2u}	2.707	497	57120	35.67	1 $^3A_{2u}$	25.90	3 $^3T_{2u}$	19.18	3 $^3T_{1u}$		
7 E_u	2.708	497	57250	31.13	3 $^3T_{1u}$	17.46	4 $^3T_{1u}$	15.57	3 $^3T_{2u}$	12.03	4 $^3T_{2u}$
				11.53	2 ^1E_u						
8 T_{1u}	2.704	494	57660	43.90	2 $^1T_{1u}$	19.09	3 $^3T_{2u}$	11.40	4 $^3T_{2u}$	10.24	2 ^3E_u
10 T_{2u}	2.707	497	57660	33.68	3 $^3T_{1u}$	29.41	1 $^3A_{2u}$				
3 A_{2u}	2.708	497	58260	59.43	3 $^3T_{2u}$	15.94	2 $^3T_{2u}$	13.18	1 $^1A_{2u}$	11.35	4 $^3T_{2u}$
4 A_{1u}	2.708	496	58700	57.70	3 $^3T_{1u}$	25.74	1 $^1A_{1u}$	12.30	4 $^3T_{1u}$		
9 T_{1u}	2.708	496	58770	52.43	2 ^3E_u	15.02	4 $^3T_{1u}$	13.13	3 $^3T_{1u}$		
8 E_u	2.707	495	58940	73.29	4 $^3T_{1u}$	15.02	3 $^3T_{1u}$				
10 T_{1u}	2.708	496	59010	44.22	3 $^3T_{2u}$	18.83	1 $^3A_{1u}$	11.07	2 $^1T_{1u}$		
11 T_{1u}	2.708	496	59420	50.23	4 $^3T_{2u}$	26.54	3 ^3E_u	12.76	2 $^1T_{1u}$		
11 T_{2u}	2.708	497	59530	58.77	3 $^3T_{2u}$	18.31	1 $^3A_{2u}$	12.77	3 $^3T_{1u}$		
9 E_u	2.708	496	59900	54.00	3 $^3T_{2u}$	35.84	3 $^3T_{1u}$				
12 T_{2u}	2.708	496	60160	24.44	3 $^1T_{2u}$	19.20	3 ^3E_u	19.10	2 ^3E_u	18.52	3 $^3T_{1u}$
				13.81	4 $^3T_{1u}$						
12 T_{1u}	2.708	495	60220	40.11	1 $^3A_{1u}$	28.20	3 $^3T_{1u}$	19.27	3 $^3T_{2u}$		
10 E_u	2.708	496	60490	78.32	4 $^3T_{2u}$	10.56	2 ^1E_u				
13 T_{1u}	2.708	495	60820	51.52	4 $^3T_{1u}$	24.97	2 ^3E_u				
13 T_{2u}	2.708	495	60830	73.72	4 $^3T_{2u}$	13.65	3 ^3E_u				
5 A_{1u}	2.708	496	60850	72.34	4 $^3T_{1u}$	14.31	3 $^3T_{1u}$	12.84	5 $^3T_{1u}$		
4 A_{2u}	2.707	495	61200	58.79	4 $^3T_{2u}$	20.87	3 $^3T_{2u}$	17.41	1 $^1A_{2u}$		
14 T_{2u}	2.708	496	61320	32.38	2 ^3E_u	25.74	3 $^1T_{2u}$	21.73	4 $^3T_{1u}$	11.36	3 ^3E_u
14 T_{1u}	2.708	496	61840	27.50	3 ^3E_u	27.39	5 $^3T_{1u}$	13.17	4 $^3T_{2u}$	13.10	3 $^1T_{1u}$
6 A_{1u}	2.708	495	62450	86.45	5 $^3T_{1u}$	11.96	4 $^3T_{1u}$				
15 T_{1u}	2.708	496	62650	50.45	5 $^3T_{1u}$	30.51	3 ^3E_u				
15 T_{2u}	2.708	496	62990	45.70	3 ^3E_u	27.58	3 $^1T_{2u}$	11.14	5 $^3T_{1u}$	10.55	4 $^3T_{2u}$
16 T_{1u}	2.709	496	63310	69.62	3 $^1T_{1u}$	10.76	3 ^3E_u				
5 A_{2u}	2.708	496	63760	68.16	1 $^1A_{2u}$	29.46	4 $^3T_{2u}$				
11 E_u	2.708	496	63910	94.26	5 $^3T_{1u}$						
16 T_{2u}	2.708	495	63920	82.33	5 $^3T_{1u}$						
17 T_{2u}	2.708	495	64980	91.51	4 $^1T_{2u}$						
12 E_u	2.708	496	65560	95.65	3 ^1E_u						
17 T_{1u}	2.708	495	65870	96.90	4 $^1T_{1u}$						
18 T_{1u}	2.708	494	69480	91.51	5 $^1T_{1u}$						
$4f\,6s$ submanifold											
$\langle d_{\mathrm{Pr-O},e}\rangle$=2.724±0.000; $\langle \omega_{a_{1g}}\rangle$=465±1											
13 E_u	2.724	465	100999	77.37	6 $^3T_{1u}$	22.64	5 $^3T_{2u}$				
18 T_{2u}	2.724	465	101074	79.13	6 $^3T_{1u}$	11.93	5 $^3T_{2u}$				
19 T_{1u}	2.724	465	101350	38.37	6 $^1T_{1u}$	34.02	6 $^3T_{1u}$	27.62	5 $^3T_{2u}$		
19 T_{2u}	2.724	466	101790	48.06	2 $^3A_{2u}$	33.11	5 $^3T_{2u}$	16.53	5 $^1T_{2u}$		
6 A_{2u}	2.724	465	101921	63.88	5 $^3T_{2u}$	36.13	2 $^1A_{2u}$				
7 A_{1u}	2.724	465	103790	99.99	6 $^3T_{1u}$						
20 T_{1u}	2.724	465	104040	65.64	6 $^3T_{1u}$	24.06	6 $^1T_{1u}$	10.31	5 $^3T_{2u}$		
14 E_u	2.724	466	104550	77.36	5 $^3T_{2u}$	22.64	6 $^3T_{1u}$				
20 T_{2u}	2.724	466	104696	54.95	5 $^3T_{2u}$	32.37	2 $^3A_{2u}$				

	21 T_{1u}	2.724	465	104762	62.09	5 $^3T_{2u}$	37.57	6 $^1T_{1u}$
	21 T_{2u}	2.724	465	105118	71.49	5 $^1T_{2u}$	18.97	2 $^3A_{2u}$
	7 A_{2u}	2.724	465	105129	63.87	2 $^1A_{2u}$	36.13	5 $^3T_{2u}$
Pr^{4+}								
				$4f^1$ manifold				
				$\langle d_{Pr-O,e}\rangle$=2.606±0.001; $\langle \omega_{a_{1g}} \rangle$ = 512±0				
$^2F_{5/2}$	1 Γ_{8u}	2.606	512	0 [a]	81.09	1 $^2T_{1u}$	18.89	1 $^2T_{2u}$
	1 Γ_{7u}	2.606	512	383	63.65	1 $^2A_{2u}$	36.35	1 $^2T_{2u}$
$^2F_{7/2}$	1 Γ_{6u}	2.606	512	2722	100.02	1 $^2T_{1u}$		
	2 Γ_{7u}	2.607	512	3589	63.65	1 $^2T_{2u}$	36.35	1 $^2A_{2u}$
	2 Γ_{8u}	2.607	512	3810	81.11	1 $^2T_{2u}$	18.90	1 $^2T_{1u}$
				$5d^1$ and $6s^1$ manifolds				
^2E_g	1 Γ_{8g}	2.661	429	59993	98.78	1 ^2E_g		
$^2T_{2g}$	2 Γ_{8g}	2.667	434	71492	98.77	1 $^2T_{2g}$		
	1 Γ_{7g}	2.668	433	72940	100.02	1 $^2T_{2g}$		
$^2S_0$	1 Γ_{6g}	2.747	349	107428	100.00	1 $^2A_{1g}$		

[a] The minimum-to-minimum $1E_g \rightarrow 1\ \Gamma_{8u}$ energy difference between the ground states of Pr^{3+} and Pr^{4+} is 64630 cm^{-1}.

TABLE S3: Spectroscopic constants of the clusters $(PrO_{12})^{21-}$ and $(PrO_{12})^{20-}$ embedded in $CaTiO_3$ calculated without including spin-orbit coupling, witout (SA-CASSCF) and with (MS-CASPT2) dynamic correlation: Pr–O equilibrium distance $d_{Pr-O,e}$ (Å), breathing mode harmonic vibrational frequency $\omega_{a_{1g}}$ (cm^{-1}), and minimum-to-minimum transition energie T_e (cm^{-1}). Manifold average values of $d_{Pr-O,e}$ and $\omega_{a_{1g}}$ (± their root mean square deviations) are given when meaningful.

			SA-CASSCF			MS-CASPT2		
	main config./term	state	$d_{Pr-O,e}$	$\omega_{a_{1g}}$	T_e	$d_{Pr-O,e}$	$\omega_{a_{1g}}$	T_e
Pr^{3+}	$4f^2$		2.720±0.000	539±0		2.698±0.001	502±1	
	^3H_g	$1\,^3T_{2g}$	2.720	539	0	2.698	502	0
		$1\,^3T_{1g}$	2.720	539	218	2.698	502	109
		$2\,^3T_{1g}$	2.721	539	800	2.699	503	743
		$1\,^3E_g$	2.720	539	374	2.698	502	1901
	^3F_g	$2\,^3T_{2g}$	2.720	539	5961	2.698	502	4827
		$3\,^3T_{1g}$	2.721	539	6228	2.699	503	5132
		$1\,^3A_{2g}$	2.720	539	6123	2.698	502	6393
	^1G_g	$1\,^1A_{1g}$	2.720	539	6172	2.697	502	5445
		$1\,^1E_g$	2.721	539	7425	2.699	503	6980
		$1\,^1T_{1g}$	2.720	539	7045	2.699	502	7926
		$1\,^1T_{2g}$	2.720	539	6493	2.698	502	8367
	^1D_g	$2\,^1E_g$	2.720	539	20332	2.698	501	16759
		$2\,^1T_{2g}$	2.720	539	20339	2.698	502	18812
	^1I_g	$3\,^1E_g$	2.720	539	25133	2.698	502	21870
		$2\,^1A_{1g}$	2.720	539	25344	2.698	502	21875
		$1\,^1A_{2g}$	2.720	539	25438	2.698	502	22113
	^3P_g	$4\,^3T_{1g}$	2.720	539	27167	2.698	502	23059
	^1I_g	$2\,^1T_{1g}$	2.720	539	25376	2.699	500	24486
		$3\,^1T_{2g}$	2.720	539	25050	2.699	502	24731
		$4\,^1T_{2g}$	2.721	539	25415	2.697	502	25116
	$^1S_0$	$3\,^1A_{1g}$	2.720	539	58040	2.698	502	48643
	$4f5de_g$		2.723±0.001	537±1		2.702±0.001	495±1	
		$1\,^1T_{2u}$	2.722	537	50465	2.701	494	47984
		$1\,^1E_u$	2.723	536	51614	2.702	496	48629
		$1\,^3T_{1u}$	2.721	537	52069	2.701	495	49929
		$1\,^3T_{2u}$	2.721	536	52568	2.701	494	50633
		$1\,^1T_{1u}$	2.725	537	53533	2.704	495	50786
		$2\,^1T_{2u}$	2.723	536	56592	2.703	495	51535
		$1\,^3E_u$	2.721	536	54270	2.701	494	51728
		$2\,^3T_{1u}$	2.723	537	54742	2.702	495	52277
		$2\,^3T_{2u}$	2.722	537	54739	2.702	494	52486
		$2\,^1T_{1u}$	2.724	537	59229	2.702	495	55125
	$4f5dt_{2g}$		2.728±0.001	538±1		2.708±0.001	496±1	
		$1\,^1A_{1u}$	2.729	539	54780	2.709	497	53675
		$2\,^1E_u$	2.727	539	58013	2.708	498	54030
		$1\,^3A_{2u}$	2.728	538	56222	2.708	497	54933
		$3\,^3T_{1u}$	2.728	539	57818	2.708	496	55608
		$3\,^3T_{2u}$	2.729	539	57907	2.709	497	56049
		$2\,^3E_u$	2.728	538	58637	2.708	497	56425
		$4\,^3T_{1u}$	2.729	539	59096	2.709	496	56610
		$1\,^3A_{1u}$	2.729	539	59442	2.709	497	56964
		$4\,^3T_{2u}$	2.728	539	61281	2.708	496	57872
		$3\,^1T_{2u}$	2.728	539	61750	2.707	496	58558
		$3\,^3E_u$	2.729	539	62001	2.709	497	59027
		$1\,^1A_{2u}$	2.729	538	62595	2.709	495	59898
		$3\,^1T_{1u}$	2.723	537	65439	2.703	495	59979
		$5\,^3T_{1u}$	2.728	538	64937	2.708	496	60577
		$4\,^1T_{2u}$	2.728	538	67681	2.708	496	62086
		$3\,^1E_u$	2.729	538	68816	2.708	496	62784
		$4\,^1T_{1u}$	2.729	538	68924	2.709	495	63111

		$5\,^1T_{1u}$	2.730	538	71225	2.709	494	66214
	$4f\,6s$		2.749±0.001	518±1		2.724±0.000	461±1	
		$6\,^3T_{1u}$	2.748	518	109407	2.724	465	99624
		$6\,^1T_{1u}$	2.748	516	110380	2.724	463	100444
		$2\,^3A_{2u}$	2.749	519	109685	2.724	465	100510
		$5\,^3T_{2u}$	2.749	519	110191	2.725	466	100650
		$2\,^1A_{2u}$	2.748	517	110743	2.724	464	101131
		$5\,^1T_{2u}$	2.749	517	111172	2.724	465	101352
Pr^{4+}	$4f^1$	$1\,^2T_{1u}$	2.626	554	66832	2.606	512	63481
		$1\,^2A_{2u}$	2.626	554	66963	2.606	512	63630
		$1\,^2T_{2u}$	2.626	554	68122	2.607	512	65097
	$5de_g^1$	$1\,^2E_g$	2.634	542	162653	2.661	429	127625
	$5dt_{2g}^1$	$1\,^2T_{2g}$	2.641	540	167916	2.668	433	139626
	$6s^1$	$1\,^2A_{1g}$	2.667	494	229594	2.747	349	174946

TABLE S4: Spectroscopic constants and analyses of the spin-orbit wave functions of the electronic states of Pr^{3+} and Pr^{4+} at the Ti site of $CaTiO_3$. Pr–O equilibrium distances $d_{Pr-O,e}$ (Å), breathing mode harmonic vibrational frequencies $\omega_{a_{1g}}$ (cm^{-1}), and minimum-to-minimum transition energies T_e (cm^{-1}). The analysis of the spin-orbit wave functions corresponds to d_{Pr-O}=2.05 Å. Manifold averages and mean square deviations are indicated when meaningful. See Fig. S4.

	State	$d_{Pr-O,e}$	$\omega_{a_{1g}}$	T_e	weights (%) of terms larger than 10%							
Pr^{3+}												
					$4f^2$ manifold							
$^3H_4$	$1\,A_{1g}$	2.067	1183	0	97.84	$1\,^3T_{1g}$						
	$1\,T_{1g}$	2.067	1183	929	88.36	$1\,^3T_{1g}$						
	$1\,E_g$	2.067	1183	1841	39.49	$1\,^3T_{2g}$	34.52	$1\,^3T_{1g}$	22.96	$2\,^3T_{1g}$		
	$1\,T_{2g}$	2.067	1178	2945	81.97	$2\,^3T_{1g}$						
$^3H_5$	$2\,T_{2g}$	2.067	1189	3166	79.93	$1\,^3T_{1g}$	11.89	$1\,^3T_{2g}$				
	$2\,E_g$	2.067	1185	3529	63.53	$2\,^3T_{1g}$	34.41	$1\,^3T_{1g}$				
	$2\,T_{1g}$	2.068	1188	3922	81.13	$1\,^3T_{2g}$						
	$3\,T_{1g}$	2.067	1183	4961	84.13	$2\,^3T_{1g}$						
$^3H_6$	$3\,E_g$	2.067	1186	5436	58.13	$1\,^3T_{2g}$	30.40	$1\,^3T_{1g}$	10.63	$2\,^3T_{1g}$		
	$2\,A_{1g}$	2.067	1183	5773	91.45	$2\,^3T_{1g}$						
	$3\,T_{2g}$	2.067	1186	5984	83.24	$1\,^3T_{2g}$	11.88	$1\,^3T_{1g}$				
	$1\,A_{2g}$	2.067	1187	6515	97.39	$1\,^3T_{2g}$						
	$4\,T_{2g}$	2.068	1191	7985	64.77	$1\,^3E_g$	17.89	$3\,^3T_{1g}$				
	$4\,T_{1g}$	2.068	1192	8184	85.99	$1\,^3E_g$						
$^3F_2$	$4\,E_g$	2.068	1184	8564	56.09	$2\,^3T_{2g}$	23.21	$1\,^1E_g$	17.90	$3\,^3T_{1g}$		
	$5\,T_{2g}$	2.069	1188	9042	72.05	$2\,^3T_{2g}$						
$^1G_4$	$3\,A_{1g}(^1G_4)$	2.067	1178	9599	83.14	$1\,^1A_{1g}$						
$^3F_3$	$2\,A_{2g}(^3F_3)$	2.068	1188	9699	97.54	$2\,^3T_{2g}$						
$^3F_4$	$5\,T_{1g}$	2.068	1186	9862	90.21	$2\,^3T_{2g}$						
	$5\,E_g$	2.060	1193	9868	53.98	$3\,^3T_{1g}$	44.24	$1\,^1E_g$				
	$6\,T_{2g}$	2.070	1194	10755	71.54	$3\,^3T_{1g}$	12.70	$2\,^3T_{2g}$	11.52	$1\,^3E_g$		
	$6\,T_{1g}$	2.069	1186	11312	67.22	$3\,^3T_{1g}$	26.32	$1\,^1T_{1g}$				
	$6\,E_g$	2.068	1190	12212	41.95	$2\,^3T_{2g}$	29.22	$1\,^1E_g$	27.08	$3\,^3T_{1g}$		
	$7\,T_{2g}$	2.069	1191	12387	85.17	$1\,^3A_{2g}$						
	$4\,A_{1g}$	2.069	1197	12419	92.27	$3\,^3T_{1g}$						
	$7\,T_{1g}$	2.067	1192	13563	67.37	$1\,^1T_{1g}$	22.89	$3\,^3T_{1g}$				
	$8\,T_{2g}$	2.068	1188	17292	90.63	$1\,^1T_{2g}$						
$^1D_2$	$7\,E_g$	2.068	1189	22289	90.59	$2\,^1E_g$						
	$9\,T_{2g}$	2.065	1180	22876	90.12	$2\,^1T_{2g}$						
$^1I_6$	$5\,A_{1g}$	2.067	1186	23846	98.96	$2\,^1A_{1g}$						
$^3P_0$	$6\,A_{1g}$	2.068	1189	26191	98.54	$4\,^3T_{1g}$						
$^3P_1$	$8\,T_{1g}$	2.068	1189	26825	99.59	$4\,^3T_{1g}$						
	$3\,A_{2g}$	2.068	1188	27049	99.82	$1\,^1A_{2g}$						
$^3P_2$	$8\,E_g$	2.068	1189	27929	87.53	$4\,^3T_{1g}$						
	$10\,T_{2g}$	2.067	1185	28036	91.36	$4\,^3T_{1g}$						
	$9\,T_{1g}$	2.065	1185	28261	99.30	$2\,^1T_{1g}$						
	$11\,T_{2g}$	2.065	1186	28575	99.62	$3\,^1T_{2g}$						
	$9\,E_g$	2.071	1197	30448	95.30	$3\,^1E_g$						
	$12\,T_{2g}$	2.068	1191	33685	99.48	$4\,^1T_{2g}$						
$^1S_0$	$7\,A_{1g}$	2.067	1186	51762	98.96	$3\,^1A_{1g}$						
					$4f^15dt_{2g}$ submanifold							
	$1\,E_u$	2.058	1191	29941	70.71	$1\,^3T_{1u}$	22.35	$1\,^3T_{2u}$				
	$1\,A_{1u}$	2.059	1187	30149	77.00	$1\,^1A_{1u}$	19.70	$1\,^3T_{1u}$				
	$1\,T_{2u}$	2.058	1191	30203	81.42	$1\,^3T_{1u}$	10.99	$1\,^3T_{2u}$				
	$1\,T_{1u}$	2.059	1185	30786	40.14	$1\,^3T_{1u}$	36.26	$1\,^1T_{1u}$	13.51	$1\,^3A_{1u}$		
	$2\,T_{1u}$	2.058	1195	31326	52.56	$1\,^3T_{2u}$	27.35	$1\,^3T_{1u}$	17.54	$1\,^1T_{1u}$		
	$1\,A_{2u}$	2.059	1194	31885	94.95	$1\,^3T_{2u}$						
	$2\,T_{2u}$	2.059	1192	32089	77.63	$1\,^3T_{2u}$						
	$2\,E_u$	2.060	1189	32278	48.67	$1\,^1E_u$	17.31	$1\,^3T_{2u}$	16.15	$2\,^3T_{1u}$	14.16	$1\,^3T_{1u}$
	$2\,A_{1u}$	2.057	1192	32580	65.14	$1\,^3T_{1u}$	19.21	$1\,^1A_{1u}$	13.45	$2\,^3T_{1u}$		
	$3\,T_{1u}$	2.059	1189	33236	26.22	$1\,^3A_{1u}$	23.04	$1\,^3T_{1u}$	18.89	$2\,^3T_{1u}$	13.99	$1\,^3E_u$
					11.25	$1\,^3T_{2u}$						
	$3\,E_u$	2.058	1194	33308	55.45	$1\,^3T_{2u}$	15.08	$1\,^1E_u$	12.28	$1\,^3T_{1u}$	10.92	$2\,^3T_{1u}$

3 T_{2u}	2.059	1191	33394	71.22	2 $^3T_{1u}$	11.55	2 ^3E_u	10.81	1 $^1T_{2u}$			
4 T_{1u}	2.059	1190	33745	37.39	1 $^1T_{1u}$	22.25	1 $^3T_{2u}$	20.57	1 $^3A_{1u}$			
4 E_u	2.059	1193	34531	67.70	2 $^3T_{1u}$	22.71	1 ^1E_u					
4 T_{2u}	2.059	1188	34586	54.70	1 ^3E_u	23.20	1 $^1T_{2u}$					
5 T_{1u}	2.058	1190	34720	28.11	2 $^3T_{1u}$	26.88	1 ^3E_u	25.32	1 $^3A_{1u}$			
3 A_{1u}	2.059	1193	35037	80.03	2 $^3T_{1u}$	15.11	1 $^3T_{1u}$					
6 T_{1u}	2.059	1191	35097	37.23	1 ^3E_u	27.12	2 $^3T_{1u}$					
5 T_{2u}	2.060	1188	35556	31.03	1 $^3A_{2u}$	24.68	1 ^3E_u	23.67	1 $^1T_{2u}$	11.27	2 $^3T_{1u}$	
7 T_{1u}	2.060	1190	36733	35.11	2 ^3E_u	27.59	3 $^3T_{1u}$	22.90	2 $^1T_{1u}$			
6 T_{2u}	2.060	1197	36901	51.96	1 $^3A_{2u}$	25.40	1 $^1T_{2u}$					
4 A_{1u}	2.062	1201	37010	92.20	3 $^3T_{1u}$							
7 T_{2u}	2.061	1195	37734	70.78	2 ^3E_u	10.63	3 $^3T_{1u}$					
8 T_{1u}	2.061	1198	37950	49.41	3 $^3T_{1u}$	22.55	2 $^3T_{2u}$	13.85	2 $^1T_{1u}$			
5 E_u	2.062	1198	38068	62.31	2 $^3T_{2u}$	22.60	2 ^1E_u					
9 T_{1u}	2.061	1197	38196	41.66	2 ^3E_u	37.69	2 $^3T_{2u}$	13.96	3 $^3T_{1u}$			
2 A_{2u}	2.061	1197	38304	50.73	2 $^3T_{2u}$	44.34	1 $^1A_{2u}$					
8 T_{2u}	2.062	1198	38328	42.07	2 $^1T_{2u}$	34.36	3 $^3T_{1u}$					
10 T_{1u}	2.060	1195	38629	58.28	2 $^1T_{1u}$	20.19	2 $^3T_{2u}$	13.42	2 ^3E_u			
6 E_u	2.060	1200	38622	58.75	2 ^1E_u	28.21	2 $^3T_{2u}$					
7 E_u	2.061	1201	39204	81.43	3 $^3T_{1u}$	15.66	2 ^1E_u					
9 T_{2u}	2.060	1200	39194	86.19	2 $^3T_{2u}$							
10 T_{2u}	2.061	1198	40028	44.89	3 $^3T_{1u}$	43.64	2 $^1T_{2u}$	10.09	2 ^3E_u			
3 A_{2u}	2.061	1196	40686	52.48	1 $^1A_{2u}$	47.39	2 $^3T_{2u}$					
11 T_{1u}	2.060	1194	42914	93.64	3 $^1T_{1u}$							
$4f^1\phi_{ITE,a_{1g}}$ submanifold												
4 A_{2u}	2.031	1154	64103	59.97	2 $^1A_{2u}$	40.03	3 $^3T_{2u}$					
11 T_{2u}	2.031	1154	64112	59.57	2 $^3A_{2u}$	26.62	3 $^3T_{2u}$	13.80	3 $^1T_{2u}$			
12 T_{2u}	2.033	1161	66092	57.96	3 $^1T_{2u}$	28.51	3 $^3T_{2u}$	13.53	4 $^3T_{1u}$			
8 E_u	2.033	1163	66106	86.39	3 $^3T_{2u}$	13.62	4 $^3T_{1u}$					
12 T_{1u}	2.033	1162	66107	86.41	3 $^3T_{2u}$							
13 T_{2u}	2.031	1158	67202	40.41	2 $^3A_{2u}$	40.31	3 $^3T_{2u}$	19.27	3 $^1T_{2u}$			
5 A_{2u}	2.031	1157	67199	59.96	3 $^3T_{2u}$	40.03	2 $^1A_{2u}$					
14 T_{2u}	2.035	1171	70522	86.47	4 $^3T_{1u}$							
9 E_u	2.035	1172	70523	86.37	4 $^3T_{1u}$	13.62	3 $^3T_{2u}$					
13 T_{1u}	2.035	1170	70537	57.17	4 $^1T_{1u}$	29.22	4 $^3T_{1u}$	13.60	3 $^3T_{2u}$			
5 A_{1u}	2.035	1170	71684	99.98	4 $^3T_{1u}$							
14 T_{1u}	2.035	1169	71690	66.24	4 $^3T_{1u}$	33.77	4 $^1T_{1u}$					
$4f^1\phi_{ITE,e_g}$ submanifold												
10 E_u	2.037	1030	79353	69.42	3 ^1E_u	15.54	4 $^3T_{2u}$	15.01	5 $^3T_{1u}$			
15 T_{2u}	2.037	1023	79405	70.37	3 ^3E_u	16.13	5 $^3T_{1u}$					
15 T_{1u}	2.037	1036	79423	71.84	3 ^3E_u	17.18	4 $^3T_{2u}$					
11 E_u	2.040	1008	81718	45.34	5 $^3T_{1u}$	41.74	4 $^3T_{2u}$					
6 A_{2u}	2.040	1015	81734	86.41	4 $^3T_{2u}$	13.57	5 $^3T_{2u}$					
16 T_{2u}	2.040	987	81763	71.91	4 $^3T_{2u}$	11.05	5 $^3T_{1u}$					
16 T_{1u}	2.039	1020	81860	50.07	5 $^3T_{1u}$	36.64	4 $^3T_{2u}$					
17 T_{2u}	2.040	1001	81895	42.30	4 $^1T_{2u}$	42.17	5 $^3T_{1u}$					
6 A_{1u}	2.039	1031	81931	85.23	5 $^3T_{1u}$	14.77	6 $^3T_{1u}$					
17 T_{1u}	2.038	1037	82181	31.54	5 $^3T_{1u}$	27.12	4 $^3T_{2u}$	19.75	5 $^1T_{1u}$	11.20	6 $^3T_{1u}$	
12 E_u	2.038	1029	82644	36.35	4 $^3T_{2u}$	33.08	5 $^3T_{1u}$	30.56	3 ^1E_u			
18 T_{2u}	2.038	1016	82747	34.11	4 $^1T_{2u}$	28.47	3 ^3E_u	24.34	5 $^3T_{1u}$	12.68	4 $^3T_{2u}$	
18 T_{1u}	2.036	1039	82986	57.59	5 $^1T_{1u}$	19.30	3 ^3E_u	13.52	4 $^3T_{2u}$			
7 A_{1u}	2.044	999	86023	85.23	6 $^3T_{1u}$	14.77	5 $^3T_{1u}$					
7 A_{2u}	2.044	1024	86103	86.41	5 $^3T_{2u}$	13.57	4 $^3T_{2u}$					
19 T_{2u}	2.043	1012	86166	67.24	5 $^3T_{2u}$	18.28	6 $^3T_{1u}$					
13 E_u	2.043	1021	86179	47.33	5 $^3T_{2u}$	39.76	6 $^3T_{1u}$					
19 T_{1u}	2.043	1022	86190	70.29	6 $^3T_{1u}$	14.43	5 $^1T_{1u}$					
20 T_{2u}	2.042	1021	86373	43.22	5 $^1T_{2u}$	34.39	6 $^3T_{1u}$	10.98	5 $^3T_{2u}$			
20 T_{1u}	2.042	1015	86468	63.08	5 $^3T_{2u}$	21.48	6 $^1T_{1u}$					
14 E_u	2.043	1022	87275	54.12	6 $^3T_{1u}$	45.86	5 $^3T_{2u}$					
21 T_{2u}	2.043	1013	87449	49.13	5 $^1T_{2u}$	40.93	6 $^3T_{1u}$					
21 T_{1u}	2.043	1079	87704	70.58	6 $^1T_{1u}$	19.81	5 $^3T_{2u}$					

Pr^{4+}

					$4f^1$ manifold			
$^2F_{5/2}$	1 Γ_{7u}	2.019	1148	0 [a]	80.19	1 $^2A_{2u}$	19.81	1 $^2T_{2u}$
	1 Γ_{8u}	2.020	1152	3336	87.65	1 $^2T_{2u}$	12.35	1 $^2T_{1u}$
$^2F_{7/2}$	2 Γ_{7u}	2.020	1152	3850	80.19	1 $^2T_{2u}$	19.81	1 $^2A_{2u}$
	2 Γ_{8u}	2.023	1163	7979	87.64	1 $^2T_{1u}$	12.35	1 $^2T_{2u}$
	1 Γ_{6u}	2.023	1161	9126	100.02	1 $^2T_{1u}$		

[a] The minimum-to-minimum $1A_{1g} \rightarrow 1\ \Gamma_{7u}$ energy difference between the ground states of Pr^{3+} and Pr^{4+} is -49590 cm^{-1}.

TABLE S5: Spectroscopic constants of the clusters $(PrO_6)^{9-}$ and $(PrO_6)^{8-}$ embedded in $CaTiO_3$ calculated without including spin-orbit coupling, witout (SA-CASSCF) and with (MS-CASPT2) dynamic correlation: Pr–O equilibrium distance $d_{Pr-O,e}$ (Å), breathing mode harmonic vibrational frequency $\omega_{a_{1g}}$ (cm^{-1}), and minimum-to-minimum transition energie T_e (cm^{-1}).

			SA-CASSCF			MS-CASPT2		
	main character	state	$d_{Pr-O,e}$	$\omega_{a_{1g}}$	T_e	$d_{Pr-O,e}$	$\omega_{a_{1g}}$	T_e
Pr^{3+}	$4f^2$							
	^3H_g	$1\,^3T_{1g}$	2.087	1221	0	2.066	1182	0
		$2\,^3T_{1g}$	2.088	1221	1992	2.067	1184	1916
		$1\,^3T_{2g}$	2.089	1225	1574	2.068	1188	2377
		$1\,^3E_g$	2.089	1227	2615	2.069	1192	5322
	^1G_g	$1\,^1A_{1g}$	2.087	1218	6530	2.066	1180	6866
	^3F_g	$2\,^3T_{2g}$	2.089	1226	7818	2.068	1189	7467
		$1\,^1E_g$	2.088	1222	7058	2.067	1186	7599
		$3\,^3T_{1g}$	2.090	1230	7505	2.070	1196	8350
		$1\,^3A_{2g}$	2.089	1227	8670	2.069	1191	9856
		$1\,^1T_{1g}$	2.088	1221	7068	2.065	1181	10152
		$1\,^1T_{2g}$	2.087	1221	9395	2.065	1179	14207
	^1D_g	$2\,^1T_{2g}$	2.089	1227	19694	2.068	1188	20049
		$2\,^1E_g$	2.089	1225	22829	2.068	1189	20562
	^1I_g	$2\,^1A_{1g}$	2.087	1223	24162	2.067	1186	21273
		$1\,^1A_{2g}$	2.089	1225	26779	2.068	1188	24503
	^3P_g	$4\,^3T_{1g}$	2.088	1225	27904	2.068	1190	24707
		$2\,^1T_{1g}$	2.087	1222	24518	2.065	1183	25700
		$3\,^1T_{2g}$	2.087	1222	24894	2.065	1183	26028
		$3\,^1E_g$	2.091	1231	28441	2.071	1197	27763
		$4\,^1T_{2g}$	2.090	1228	27856	2.068	1191	31118
	^1S_g	$3\,^1A_{1g}$	2.087	1223	57673	2.067	1186	48989
	$4f5dt_{2g}$							
		$1\,^1A_{1u}$	2.083	1213	31526	2.059	1186	28337
		$1\,^3T_{1u}$	2.083	1216	33486	2.057	1192	28905
		$1\,^1T_{1u}$	2.085	1207	35438	2.060	1187	29829
		$1\,^3T_{2u}$	2.084	1219	34413	2.058	1194	29940
		$1\,^1E_u$	2.084	1216	35660	2.060	1188	30756
		$1\,^3A_{1u}$	2.083	1214	35895	2.059	1186	31278
		$2\,^3T_{1u}$	2.085	1219	37539	2.058	1193	31867
		$1\,^3E_u$	2.083	1213	36837	2.059	1187	32565
		$1\,^1T_{2u}$	2.084	1207	38622	2.060	1187	33175
		$1\,^3A_{2u}$	2.084	1220	36160	2.062	1194	33560
		$2\,^3E_u$	2.084	1220	38862	2.062	1194	34871
		$2\,^1T_{1u}$	2.083	1207	43271	2.059	1189	35470
		$3\,^3T_{1u}$	2.086	1225	40724	2.061	1202	35640
		$2\,^3T_{2u}$	2.087	1226	40694	2.061	1201	35813
		$2\,^1E_u$	2.084	1214	42556	2.060	1192	35915
		$2\,^1T_{2u}$	2.086	1212	43149	2.062	1196	36258
		$1\,^1A_{2u}$	2.084	1218	40608	2.061	1192	36842
		$3\,^1T_{1u}$	2.084	1213	47277	2.060	1194	39991
	$4f\phi_{ITE,a_{1g}}$							
		$2\,^1A_{2u}$	2.052	1218	74820	2.030	1150	62788
		$2\,^3A_{2u}$	2.052	1223	74661	2.031	1150	62807
		$3\,^1T_{2u}$	2.054	1197	75729	2.032	1159	63910
		$3\,^3T_{2u}$	2.052	1243	75730	2.032	1163	63933
		$4\,^3T_{1u}$	2.054	1242	78999	2.035	1171	68032
		$4\,^1T_{1u}$	2.056	1203	79146	2.035	1168	68053
	$4f\phi_{ITE,e_g}$							
		$3\,^1E_u$	2.060	1006	87752	2.036	1038	77795
		$3\,^3E_u$	2.063	982	87326	2.037	1039	77827

		$4\,^3T_{2u}$	2.062	993	88417	2.039	1026	79551
		$5\,^3T_{1u}$	2.067	982	87938	2.040	1007	79660
		$4\,^1T_{2u}$	2.062	967	88521	2.038	963	79878
		$5\,^1T_{1u}$	2.052	1157	89579	2.035	1056	80448
		$5\,^3T_{2u}$	2.071	966	91156	2.045	1012	83605
		$6\,^3T_{1u}$	2.066	1003	91512	2.043	1024	83625
		$5\,^1T_{2u}$	2.062	1058	91897	2.043	1001	84051
		$6\,^1T_{1u}$	2.053	1178	93003	2.038	1079	84448
Pr^{4+}	$4f^1$	$1\,^2A_{2u}$	2.038	1183	-50718	2.018	1148	-51389
		$1\,^2T_{2u}$	2.039	1187	-48361	2.020	1153	-48517
		$1\,^2T_{1u}$	2.042	1194	-44966	2.024	1162	-44067
	$5dt^1_{2g}$	$1\,^2T_{2g}$	2.030	1163	24587	2.010	1117	4834
	$\phi_{ITE,a_{1g}}$	$1\,^2A_{1g}$	1.996	1259	71221	1.979	1250	32247
	ϕ_{ITE,e_g}	$1\,^2E_g$	2.024	799	84919	1.991	1097	48408